materials

MDPI

Article

Selected Shear Models Based on the Analysis of the Critical Shear Crack for Slender Concrete Beams without Shear Reinforcement

Monika Kaszubska [1,*] and Renata Kotynia [2]

[1] Department of Building Materials Physics and Sustainable Design, Faculty of Civil Engineering, Architecture and Environmental Engineering, Lodz University of Technology, Al. Politechniki 6, 93-590 Łódź, Poland
[2] Department of Concrete Structures, Faculty of Civil Engineering, Architecture and Environmental Engineering, Lodz University of Technology, Al. Politechniki 6, 93-590 Łódź, Poland
* Correspondence: monika.dymecka@p.lodz.pl

Abstract: This paper is devoted to the shear of slender concrete beams flexurally reinforced with two types of reinforcement: steel and fiber-reinforced polymer (FRP) without transversal reinforcement. The paper presents four theoretical models for calculating the shear capacity of the collected test database and the authors' own research program, which contained 29 single-span, simply supported T-section beams reinforced with steel and glass fiber-reinforcement polymer (GFRP) bars. The paper presents a comprehensive analysis of the test results and modeling of design shear capacity in accordance with the selected theoretical models. The generalized assessment of computational analysis confirmed compatibility of the predicted and experimental results.

Keywords: shear; FRP reinforcement; test; concrete beams; modeling; slenderness; failure mode

Citation: Kaszubska, M.; Kotynia, R. Selected Shear Models Based on the Analysis of the Critical Shear Crack for Slender Concrete Beams without Shear Reinforcement. *Materials* **2022**, *15*, 8259. https://doi.org/10.3390/ma15228259

Academic Editor: F. Pacheco Torgal

Received: 16 September 2022
Accepted: 10 November 2022
Published: 21 November 2022

1. Introduction

New trends in fiber-reinforced polymer (FRP) reinforcement development broaden the scope of research on shear in the FRP-reinforced members. Compared to conventional steel reinforcement, FRPs differ essentially in the fully linear-elastic behavior, significantly higher tensile strength and lower modulus of elasticity (depending on the type of fibers).

The use of FRP reinforcement in real construction caused the need for the modification and development of design provisions for shear strength in FRP-reinforced members [1–5]. The design procedures for concrete structures reinforced with FRP bars usually are based on the guidelines for steel-reinforced concrete (RC) structures. The longitudinal FRP reinforcement is taken into account by introducing a stiffness reduction in the composite reinforcement in comparison with conventional steel reinforcement [1]. The basis of this modification is the assumption that the bond of FRP reinforcement to concrete is the same as that of steel. The analysis of selected design procedures for FRP members [6] shows a great variety of accuracy. In extreme cases, the calculated shear strength is almost 60% greater or three times lower than the shear strength from experimental research. The differences in test and calculated results mean there is still no general agreement on a rational theory for calculating the shear capacity members without transverse reinforcement. Following this revision, researchers look for new solutions or modification of existing ones.

The mechanism of shear failure in the support zone of RC elements is determined by many factors: sliding and rotation of both parts of the element crossed by the diagonal shear crack accompanied by the aggregate interlock action in concrete, dowel action of the longitudinal reinforcement, transfer of the shear force by the uncracked concrete in the compression zone and direct strut action for point load close to the support. The percentage of each component in the shear capacity of steel RC beams without shear reinforcement is determined as: 33–50% (effect of aggregate interlock), 20–40% (compressive concrete zone), and 15–25% (dowel action effect) [7,8]. However, some researchers suggest that in the elements without transverse reinforcement, the last-mentioned influence is insignificant due to the limitation of vertical displacements only through the concrete cover [9,10]. The current knowledge in the shear theories aims to take into account the complexity of the shear failure mechanism in the support zone and to include the influence above mentioned factors.

The shear failure modes collected from the literature and based on the own research are quite similar [6]. The flexural cracks with almost vertical arrangement occur during the initial stage of loading, then they propagate towards the support and incline in the direction of the loading point. The critical shear crack is most often created as a combination of minimum two cracks which are connected. The analysis of the development of critical shear crack and its influence on shear capacity is the main criterion to choose the four shear models available in the literature: Muttoni and Ruiz 2008 [11], Zhang et al. [12], Yang [13], and Cladera et al. [14]. These selected models take into account the mechanism governed shear capacity in the beams without stirrups, but different mechanisms are considered as decisive. In two models [13,14], the individual influence of parameters can be extracted.

The main aim of the analysis is to assess the accuracy of models and to identify the reason for differences between calculated and experimental shear strength results. It could be interesting also to indicate which shear mechanism in the calculation model gives results closer those from experimental tests.

2. Overview of Selected Theoretical Models

2.1. Muttoni and Ruiz 2008 [11]

The Critical Shear Crack Theory (CSCT) proposed by Muttoni and Ruiz [11] assumes that the shear capacity of reinforced concrete beams without stirrups depends on the crack width and roughness of the critical crack edges. The impact of the shape and location of the critical crack on each mechanism of transferring the shear force is determined.

The components of the shear mechanism in Muttoni and Ruiz's model [11] are the transfer of shear force through a piece of concrete separated by two cracks, the aggregate interlock effect, and the dowel action in the longitudinal reinforcement. The dowel action occurs mainly in beams, where the critical crack develops close to the support and in the RC beams with transverse reinforcement. In other cases, the effect of dowel action is negligible [11]. The residual tensile concrete stress is contributed to the shear force transfer in the section of the critical shear crack where the width is very small. Apart from the above-mentioned "beam mechanisms" in the CSCT model, there is the shear force transmission onto the support, with the inclined concrete chord. The arch effect is dominant in short beams, where the ratio of the distance between the load application point and the support to the effective depth is a/d < 2.5 [15]. Based on the above mentioned mechanism, Muttoni and Ruiz used the results of slender steel RC beams and proposed the empirical model presented in the following analysis (Equations (1)–(3)).

$$V_{cal} = \frac{b_w d \sqrt{f_c}}{3} \frac{1}{1 + 120 \frac{\varepsilon d}{16 + d_g}} \tag{1}$$

$$x = d \rho_l \frac{E}{E_c} \left(\sqrt{1 + \frac{2E_c}{\rho_l E}} - 1 \right) \tag{2}$$

$$\varepsilon = \frac{M}{d b_w \rho_l E \left(d - \frac{x}{3}\right)} \frac{0.6d - x}{d - x} \tag{3}$$

where: b_w is the beam's width, d is the effective depth, f_c is the compressive concrete strength, ε is the concrete strain, d_g is the maximum aggregate size, x is the neutral axis depth, $\rho_l = A_l/(b_w d)$ is the longitudinal reinforcement ratio, E is the modulus of elasticity of longitudinal reinforcement, E_c is the elasticity modulus of concrete, M is the bending moment in the critical section; the critical section is located $d/2$ from the load point.

2.2. Zhang et al., 2014 [12]

The advantage of the second model by Zhang et al. [12] is its possibility of use for elements without transversal reinforcement, with steel and FRP longitudinal reinforcement as reported by the authors. The main assumption is the initiation of shear with a diagonal crack, which for simplicity was assumed to form linearly. Failure occurs when the slope of this crack reaches the limit angle β_{CDC}, at which both edges of the diagonal crack start to slip. β_{CDC} is angle determined, based on the internal forces V and M acting in the cross-section:

$$\beta_{CDC} = -15\frac{M}{Vd} + 89.7^\circ \qquad \text{if} \quad \frac{M}{Vd} \leq 3.14 \tag{4}$$

$$\beta_{CDC} = 42.6^\circ \qquad \text{if} \quad \frac{M}{Vd} > 3.14 \tag{5}$$

The capacity provided by the slip of the compression zone can be determined based on shear stress, which is dependent on the compressive force in concrete and presliding shear friction failure properties A and B, depending on the type of concrete. The parameters A and B are adopted according to [16]:

$$A = 0.347{f_c}^{0.665} \tag{6}$$

$$B = \frac{0.400f_c - 0.37 - A}{0.25f_c} \tag{7}$$

Finally, the shear capacity is calculated according to formula:

$$V_{cal} = V_{cap} = \frac{bxA}{1 - [(B\sin\beta_{CDC} - \cos\beta_{CDC})\sin\beta_{CDC}] \cdot \left(\frac{M/V - d/\tan\beta_{CDC}}{z}\right)} \tag{8}$$

The neutral axis depth is determined as:

$$x = \frac{E}{E_c}\rho_l d\left(\sqrt{1 + \frac{2}{\frac{E}{E_c}\rho_l}} - 1\right) \tag{9}$$

The modulus of elasticity of concrete is adopted according to [17]:

$$E_c = 3320{f_c}^{0.5} + 6900 \tag{10}$$

Based on linear distribution of normal stresses in the compression zone, the arm of internal forces is calculated according to the following formula:

$$z = d - \frac{x}{3} \tag{11}$$

2.3. Yang 2014 [13]

Yang's model [13] is also based on the analysis of the diagonal crack development. The main crack after reaching a height z_{cr} (Equation (12)) stabilizes over the height z_{cr} and a further load increase causes only an increase in its width and crack development in the horizontal direction.

$$z_{cr} = \left(1 + \rho_l\frac{E}{E_c} - \sqrt{2\rho_l\frac{E}{E_c} + (\rho_l\frac{E}{E_c})^2}\right)d \tag{12}$$

An additional vertical displacement is needed to activate an aggregate interlock mechanism to transfer the shear forces, which arises from the development of a secondary horizontal branch of the crack at the reinforcement level. Based on the experimental results of concrete members without transversal reinforcement [13], the critical value of the vertical displacement of the diagonal Δ_{cr} is calculated according to:

$$\Delta_{cr} = \frac{25d}{30610\phi} + 0.0022 \leq 0.025\text{mm} \quad (13)$$

where ϕ is the diameter of longitudinal reinforcement.

Based on research [18], the distance between the main cracks is determined as:

$$l_{cr} = \frac{z_{cr}}{1.28} \quad (14)$$

The aggregate interlock mechanism V_{ai} in the transverse force transfer is determined based on Walraven's model [19]:

$$V_{ai} = f_c{}^{0.56} z_{cr} b_w \frac{0.03}{w - 0.01}\left(-978\Delta_{cr}{}^2 + 85\Delta_{cr} - 0.27\right) \quad (15)$$

The crack width is determined on the level of longitudinal reinforcement as:

$$w = \frac{M}{\left(\frac{2}{3}d + \frac{1}{3}z_{cr}\right)A_l E} l_{cr} \quad (16)$$

where A_l is the cross section of longitudinal reinforcement.

The dowel action force is determined according to model [20]:

$$V_d = 1.64(b_w - n\phi)\phi \sqrt[3]{f_c} \quad (17)$$

where n is the number of longitudinal reinforcement bars.

The contribution of the uncracked concrete zone in the shear capacity is determined by the assumption of Mörsch's theory [21]. As the parabolic distribution of the shear stress with the maximum value at the level of the neutral axis is assumed, the transverse force transferred through the compressive concrete zone is determined as follows:

$$V_c = \frac{2}{3} \frac{d - z_{cr}}{\left(\frac{2}{3}d + \frac{1}{3}z_{cr}\right)} V \quad (18)$$

where V is the shear force in the critical section.

According to the [13] model, the shear capacity is a sum of the shear forces transferred by the uncracked compressive chord, across the web cracks and the dowel action in the longitudinal reinforcement:

$$V_{cal} = V_c + V_{ai} + V_d \quad (19)$$

Evaluation of the maximum shear force needs iteration, since the load applied on the beam is unknown in advance. In this paper, V in Equation (18) is equal to V_{max}.

2.4. Cladera et al., 2016 [14]

The first model version by Cladera et al. [14] for rectangular beams was presented in [10]. The shear strength is calculated as a sum of the shear force transferred by the uncracked compression chord (V_c), shear transferred across web cracks (V_w) and dowel action in the longitudinal reinforcement (V_d).

The model can be used regardless of the load type (distributed, point load) [22]. The model is also developed for the slender reinforced concrete T- and I-shaped beams [23]. What is used in the presented analysis is the last version of the model [14], Equations (20)–(28).

In [14], the authors also propose a simplified version of model. In this version, due to a small impact of residual tensile stress and dowel effect, these components are incorporated into v_c. However, to show the contribution of different mechanisms in shear strength, this analysis uses Equation (20) with the sum of the shear resisted in the uncracked compression chord (v_c) and shear transferred across web cracks (v_w):

$$V_{cal} = (v_c + v_w) f_{ctm} b_{v,eff} d \tag{20}$$

$$\nu_c = \zeta \left(0.88\frac{x}{d} + 0.02\right)\frac{b_{v,eff}}{b} \tag{21}$$

$$\nu_w = 167\frac{f_{ctm}}{E_c} \cdot \frac{b_w}{b}\left(1 + \frac{2G_f E_c}{f_{ctm}^2 d}\right) \tag{22}$$

$$G_f = 0.028 f_c^{0.18} d_g^{0.32} \tag{23}$$

$$f_{ctm} = 0.30 {f_c}^{2/3} \tag{24}$$

$$x = \left(\frac{E}{E_c}\rho_l\left(-1 + \sqrt{1 + \frac{2}{\frac{E}{E_c}\rho_l}}\right)\right)d \tag{25}$$

$$x > h_f \rightarrow b_{v,eff} \approx b_w + (b_v - b_w)\left(\frac{h_f}{x}\right)^{3/2} \tag{26}$$

$$x \le h_f \rightarrow b_{v,eff} = b_v = b_w + 2h_f < b \tag{27}$$

This model considers a size effect by factor ζ:

$$\zeta = \frac{2}{\sqrt{1 + \frac{d}{200}}}\left(\frac{d}{a}\right)^{0.2} > 0.45 \tag{28}$$

where h_f is the flange height in T-section beam, a is the distance from the support to the load point.

3. Test Database

In the analysis of the above-described models, a database collected from literature and the authors' own experimental program is used. The beams with a/d > 2.8 reinforced with AFRP (aramid fibre reinforced polymer), GFRP (glass FRP), CFRP (carbon FRP), and steel failed in shear were chosen for the analysis (Figure 1, Table 1). The steel-reinforced elements were limited and included in the database only if they were analyzed in research related to the FRP-reinforced members.

All necessary parameters used in the analyzed models are not available in some experimental programs from the literature, so the number of elements for calculation of the shear capacity according to the respective models are different (the number of used members is determined in Tables 1 and 2). A very limited number of elements is used in Muttoni and Ruiz's [11] and Cladera et al.'s [14] models, due to the lack of information about the maximum aggregate size (d_g). In Yang's model [13], the lack of the reinforcement diameter in some research causes problems with the analysis.

The authors' own research program consists of 29 single-span, simply supported beams without transverse reinforcement. The three-point loaded beams with the load located at a distance a = 1100 mm from the support has the shear span to depth ratio a/d in the range of 2.9–3.0, referring to slender beams. Opposite to members collected from the literature, the cross section of beams is T-shaped (b = 400 mm, b_w = 150 mm, h_f = 60 mm, h_{tot} = 400 mm). The choice of T-section beams to our own tests is connected with two aspects: influence of cross section on shear capacity [23] and plan to continue the shear test for elements with shear reinforcement, which has been partially realized in [24,25]. The essential details of the specimens are presented in Table 1. More details of the experimental tests and analysis of the own test results were published in [26–28].

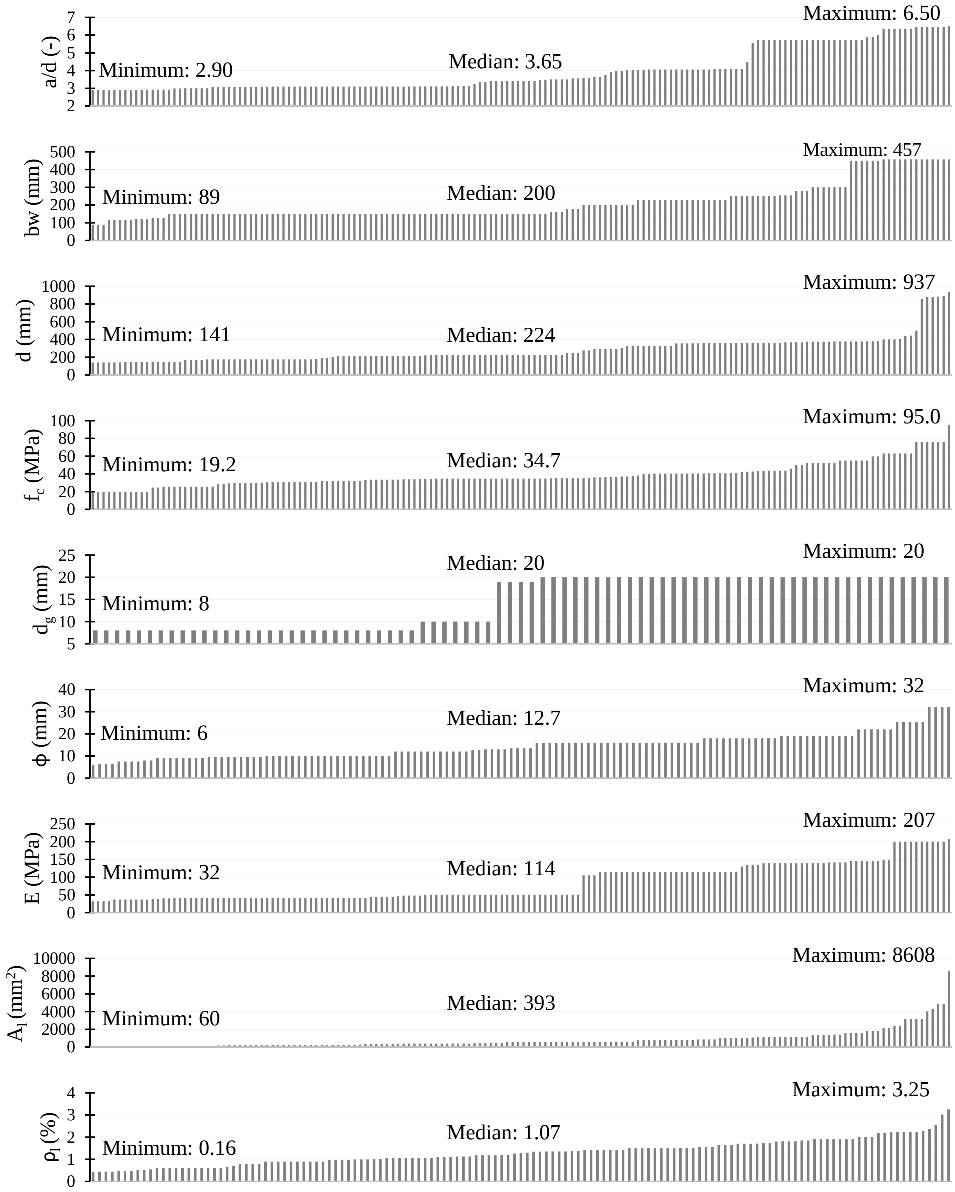

Figure 1. Characteristics of test database.

Table 1. Statistic assessment of models for all members (Table 1).

	Muttoni and Ruiz [11]	**Zhang et al. [12]**	**Yang [13]**	**Cladera et al. [14]**
Number of specimens	79	158	134	79
η_{min}	0.62	0.48	0.40	0.63
η_{max}	2.47	2.50	2.19	1.57
η_m	1.16	1.01	1.31	1.09
median	1.11	1.01	1.32	1.09
σ_η	0.35	0.27	0.31	0.18
COV	0.30	0.27	0.24	0.17

$\eta = V_{max}/V_{cal}$; η_{min}—minimum η value; η_{max}—maximum value η; η_m—medium η value; σ_η—standard deviation of η; COV—coefficient of variation of η (COV = σ_η/η_m).

Table 2. Statistic assessment of design models with divisions.

	Muttoni and Ruiz [11]	**Zhang et al. [12]**	**Yang [13]**	**Cladera et al. [14]**
	CFRP-reinforced rectangular beams			
Number of specimens	26	56	47	26
η_{min}	0.78	0.54	0.40	0.71
η_{max}	1.85	1.57	2.04	1.42
η_m	1.20	1.04	1.38	1.06
σ_η	0.26	0.20	0.32	0.17
COV	0.22	0.20	0.23	0.16
	GFRP-reinforced rectangular beams			
Number of specimens	22	60	51	22
η_{min}	0.65	0.71	0.86	0.63
η_{max}	2.47	2.50	2.19	1.57
η_m	1.37	1.16	1.39	1.05
σ_η	0.43	0.28	0.27	0.21
COV	0.31	0.24	0.19	0.20
	GFRP-reinforced T-beams			
Number of specimens	16	16	16	16
η_{min}	0.85	0.60	1.04	0.99
η_{max}	1.48	0.93	1.69	1.45
η_m	1.12	0.78	1.30	1.15
σ_η	0.18	0.10	0.18	0.11
COV	0.16	0.13	0.14	0.10
	GFRP-reinforced beams (T-section and rectangular)			
Number of specimens	38	76	67	38
η_{min}	0.65	0.60	0.86	0.63
η_{max}	2.47	2.50	2.19	1.57
η_m	1.26	1.08	1.37	1.10
σ_η	0.37	0.29	0.25	0.19
COV	0.29	0.27	0.18	0.17
	steel-reinforced rectangular beams			
Number of specimens	2	11	7	2
η_{min}	-	0.68	0.95	-
η_{max}	-	1.16	1.46	-
η_m	-	0.93	1.20	-
σ_η	-	0.15	0.22	-
COV	-	0.16	0.19	-
	steel-reinforced T-beams			
Number of specimens	13	13	13	13
η_{min}	0.67	0.48	0.70	0.96
η_{max}	1.08	0.73	1.11	1.48
η_m	0.82	0.61	0.84	1.19
σ_η	0.12	0.07	0.13	0.16
COV	0.15	0.12	0.15	0.14
	steel-reinforced beams (T-section and rectangular)			
Number of specimens	15	24	20	15
η_{min}	0.62	0.48	0.70	0.74
η_{max}	1.08	1.16	1.46	1.48
η_m	0.81	0.75	0.97	1.14
σ_η	0.13	0.20	0.24	0.19
COV	0.16	0.26	0.24	0.17

For the evaluation of the accuracy of the test and predicted results by models, the following coefficient was used: $\eta = V_{max}/V_{cal}$, where V_{max} is the maximum experimental shear force and V_{cal} is the shear force calculated according to the above presented models. The results corresponding to values of $\eta < 1$ are overestimation of the shear strength values compared to the test results. Results corresponding to $\eta > 1$ indicate lower values of the shear load capacity, which confirms the conservative approach of the verified model. A dead load was not taken into account in the calculated analysis. The mean test values of the reinforcement and concrete were used in the analysis (Table 1). In the model in [11], the value of bending moment M is assumed for a section located $d/2$ from the load point. However, in the models in [12,13], the critical section is assumed in the position of point load, according to the publications. The concrete elasticity modulus E_c is assumed according to [29], except in Zhang et al.'s model, where the authors suggest [17].

4. Results and Analysis

In the generalized assessment of accuracy of calculation models without division into a type of longitudinal reinforcement, Yang's model [13] with $\eta_m = 1.31$ is the most conservative one (Table 1). However, the Yang model also indicates the minimum value of η ($\eta_{min} = 0.40$). The most expected value of η_m close to 1 is obtained for the Zhang et al. model [12], but with 49% overestimated results (Figure 2). According to this model [12], the largest number of elements are analyzed (158 members). The lowest dispersion of calculated results is for Cladera et al.'s model [14] (COV = 17%, 79 elements) with value of $\eta_m = 1.09$. The η_m coefficient by Muttoni and Ruiz [11] is similar to [14], but COV increased to 30% for the same number of elements.

For the FRP reinforcement, models by Cladera et al. [14], Muttoni and Ruiz [11], and Zhang et al. [12] are slightly more conservative for GFRP-reinforced members ($\eta_m = 1.08$–1.26) than for the beams with CFRP reinforcement ($\eta_m = 1.04$–1.20). The η_m coefficient by Yang [13] is almost the same for CFRP and GFRP bars, respectively $\eta_m = 1.37$ and $\eta_m = 1.38$, but results for GFRP-reinforced elements are close to the mean value (COV decreased from 0.23 to 0.19, Table 2).

The AFRP reinforced beams shown in Figure 2 are not included in the statistic assessment shown in Table 2, because only two members are available. The same situation is for steel RC rectangular beams for models [11,14].

The shear capacity of steel-reinforced rectangular beams is predicted quite well with smaller dispersion of results than for FRP-reinforced members, but the number of steel RC beams is very limited in this analysis. However, the shear capacity of T-beams from the author's own experimental research is overestimated in almost all cases, the exception is model [14] (Figure 2).

The biggest overestimation of the V_{cal} of T-beams is by Zhang et al.'s model [12]. The one possible reason for this is the assumption that the top of the critical shear crack is in the point of load. In T-beams, the critical crack after reaching the shelf developed horizontally in the direction of point of load. Thus, in most beams, the top of the inclined part of the crack was located in some distance from the applied force [28]. Zhang et al. considered taking into account the change in the position of the crack, but ultimately found this influence insignificant [30]. The detailed analysis of the location shear crack in T-beams in [6] shows a slightly decrease in overestimation of V_{cal} calculated according to [12,30] with consideration of the top of critical crack shifts (η_m increases from 0.61 to 0.66). The angle of inclination of the critical crack calculated for the own test beams according to the formula (4 and 5) is similar in all members and ranges from 43° to 46°. These values differ from the angle of inclination critical crack determined on the basis of the research [6]. The reason for overestimation of shear capacity calculated based on model Zhang et al. could lie also in the empirical parameters A and B, which can be calibrated on a higher number of concrete classes and can take into account the effect of aggregate and the bond of reinforcement to various types of concrete.

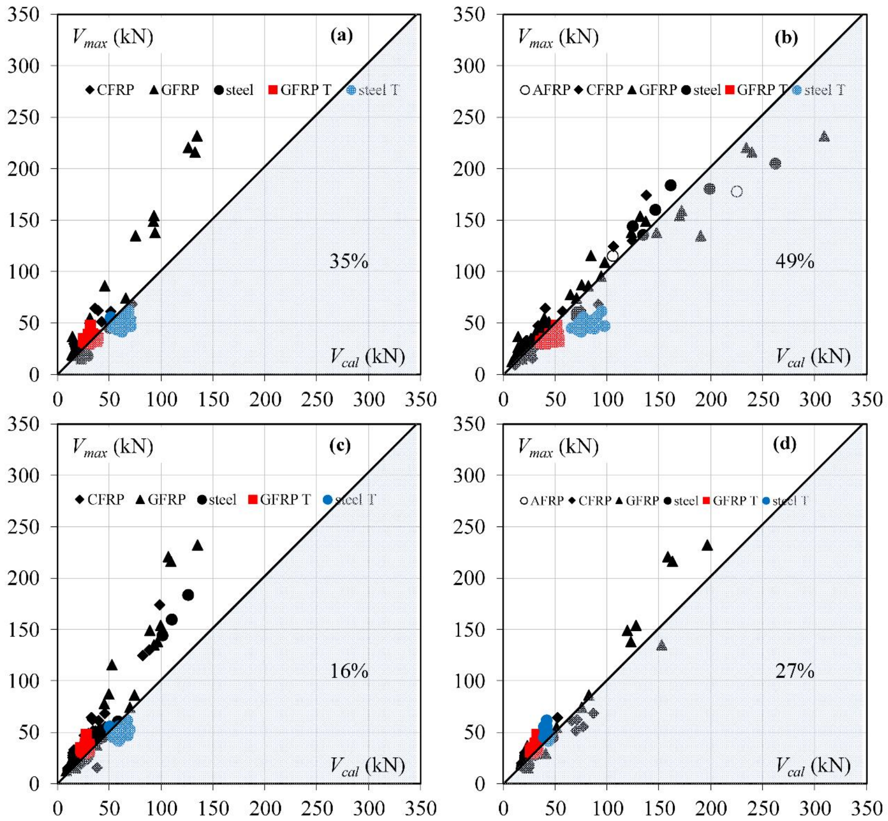

Figure 2. The comparison of experimental and calculated shear capacity according to the presented models (percentage points indicate overestimated results $V_{cal} > V_{max}$): (**a**) Muttoni and Ruiz [11], (**b**) Zhang et al. [12], (**c**) Yang [13], (**d**) Cladera et al. [14].

The comparison of the contribution of V_c, V_{ai} and V_d calculated according to Yang's model [13] for steel reinforced T-section and rectangular beams indicates that the overestimation V_{cal} in T-beams can be connected with overestimation the influence of the aggregate interlock effect. In rectangular beams, the contribution of V_{ai} is from 45% to 58%, while in T-section beams, it is from 61% to 73% (Figure 3).

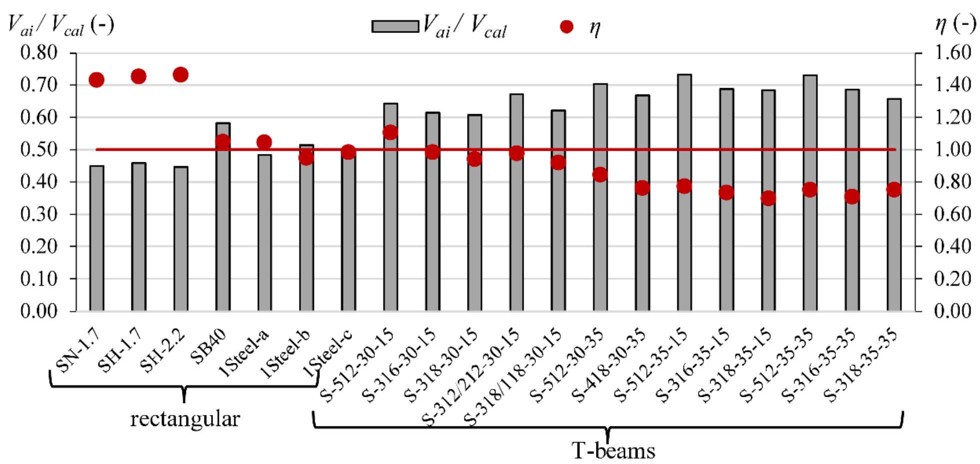

Figure 3. The contribution of the aggregate interlock effect V_{ai} in V_{cal} according to Yang's model in steel RC beams (red line indicated $\eta = 1$).

Muttoni and Ruiz's model [11] is more conservative for GFRP-reinforced T-beams confirmed by $\eta_m = 1.12$, while for steel RC beams, it is $\eta_m = 0.82$ (Table 2). In this model, one of the parameters determining the shear capacity is the concrete strain ε (Equation (3)), which depends, among others, on the modulus of elasticity of longitudinal reinforcement. The GFRP bars used in T-beams have four times lower elasticity modulus than steel reinforcement, hence the strains calculated in the GFRP-reinforced beams indicated much higher values than in the steel-reinforced members, which caused the lower design shear capacity of these beams. The confirmation of above is that also for rectangular beams with FRP reinforcement, the V_{cal} according to [11] is in most cases lower than V_{max}, with η_m = 1.20 for CFRP reinforcement and η_m = 1.37 for GFRP bars. The attempt to calibrate the Muttoni and Ruiz's model for FRP bars made in [6] does not finally allow to obtain the formula, which would describe the shear capacity of the tested elements with a satisfactory accuracy. The problem is the limited number of members, which make it possible to calibrate the model only in a certain range of variable parameters.

Theoretical models show the independence from the reinforcement ratio and concrete compressive strength. One clear tendency is not observed in Figures 4 and 5, so the shear capacity is calculated with similar accuracy. However, it is worth mentioning that most beams have the normal concrete strength, while the number of beams with the high concrete strength is limited.

Cladera et al.'s [14] and Yang's [13] models define the contribution of individual components of the shear mechanism. This influence of individual shear force mechanisms is analyzed for T-section beams from the authors' own research program and for 45 beams from the database, for which it is possible to calculate shear capacity according to both models [13] and [14]. In Cladera et al.'s [14] model, it is assumed that the shear resistance is provided by the non-cracked concrete zone ($V_{c,C}$), Equations (20) and (21), and by the aggregate interlock and residual tensile strength, which are taken together as a component of $V_{w,C}$, Equations (20) and (22). Yang's model considers three components in the shear capacity: $V_{c,Y}$—force transmitted by concrete, $V_{ai,Y}$—force transmitted by aggregate interlock, and $V_{w,Y}$—force transmitted by dowel action of longitudinal reinforcement.

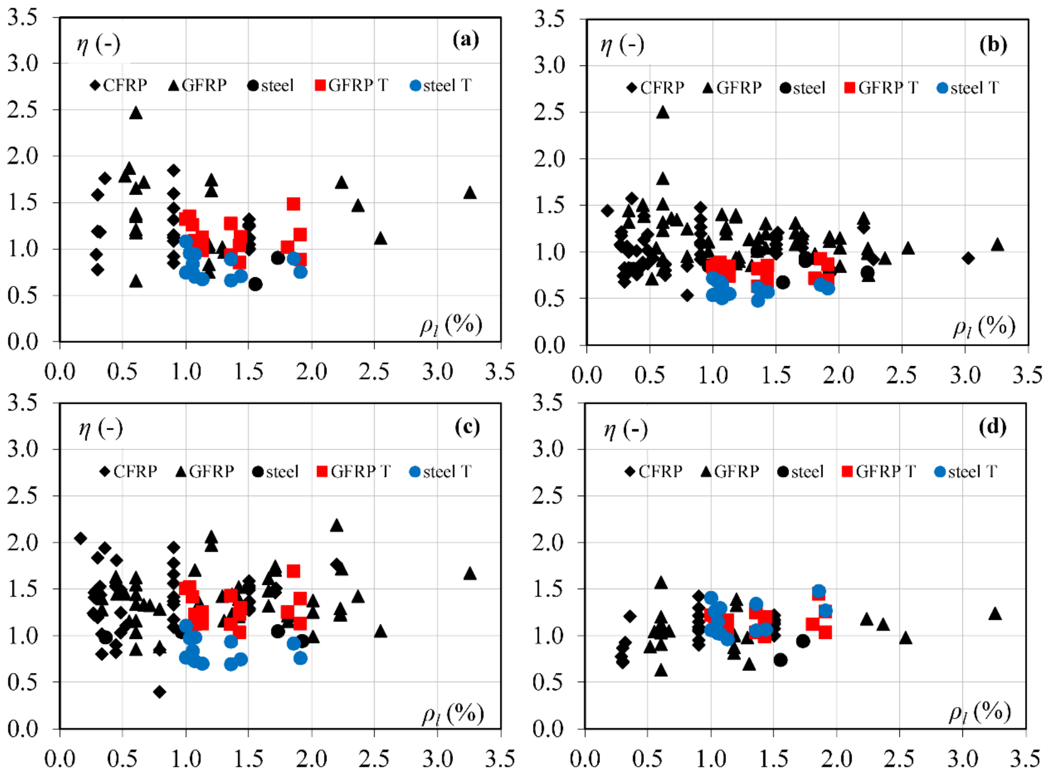

Figure 4. The influence of longitudinal reinforcement ratio on η values: (**a**) Muttoni and Ruiz [11], (**b**) Zhang et al. [12], (**c**) Yang [13], (**d**) Cladera et al. [14].

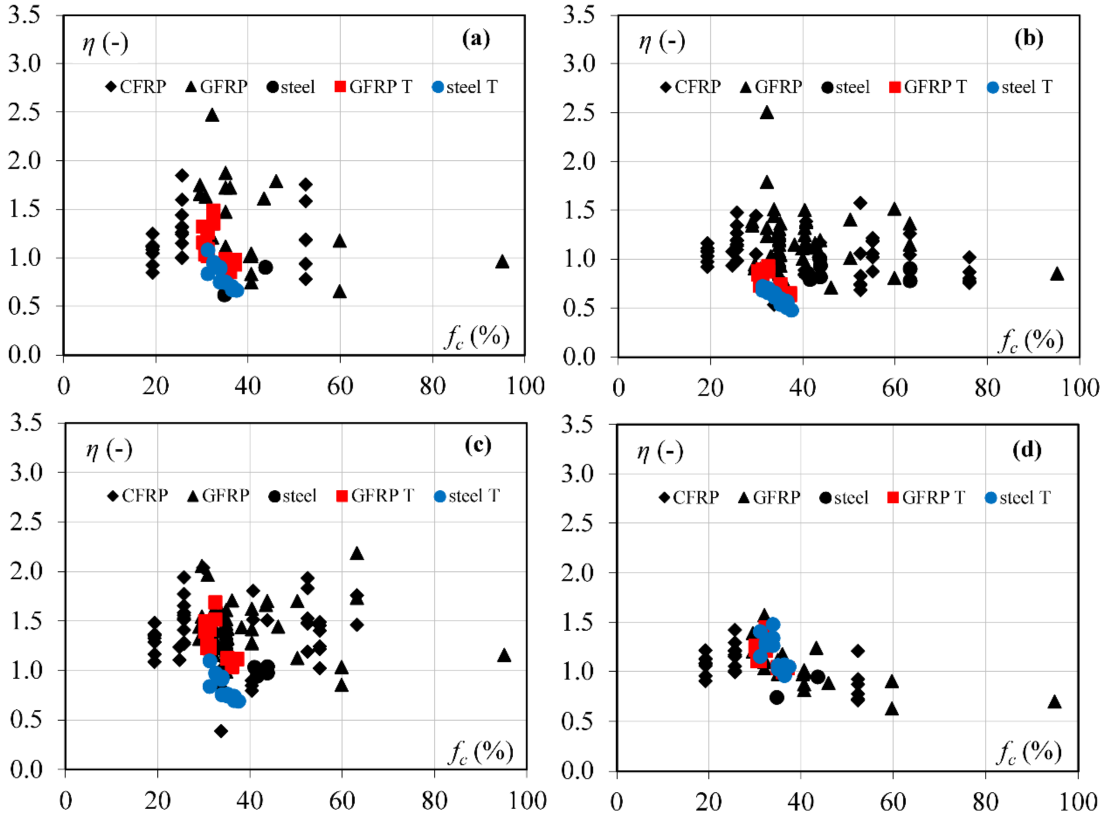

Figure 5. The influence of concrete compressive strength on η values: (**a**) Muttoni and Ruiz [11], (**b**) Zhang et al. [12], (**c**) Yang [13], (**d**) Cladera et al. [14].

The main difference between the models in [13] and [14] is the dowel action force, which is included only in Yang's model [13] and lacks in Cladera et al.'s model [14]. Cladera et al.'s model takes this effect into account, but only in members with stirrups.

The contribution of the non-cracked concrete zone V_c in calculated shear capacity for Cladera et al. model [14] is from 64% to 87% in rectangular beams and from 56% to 72% in T-section beams, whereas in Yang's model, this contribution is from 6% to 33% in rectangular beams and from 13% to 27% in T-section beams (Figures 6–11). The cause of the differences in the contribution of the non-cracked concrete zone V_c component in the shear capacity calculated according to the models in [14] and [13] is the difference in basic assumption for V_c. Cladera et al.'s model considers a biaxial stress state that occurs in the non-cracked concrete zone, and failure occurs when the principal stresses calculated based on the Mohr's model reaches the limit value according to Kupfer's law [31]. The shear stresses, calculated from the above relationships at the height of the compression zone, determine the contribution of concrete $V_{c,C}$. On the other hand, the model in [13] considers the compressive force contribution based only on the tangential stresses in the cross-section.

The contribution of the aggregate interlock action in calculated shear capacity in the model in [13] is from 9% to 58% in rectangular beams and from 48% to 73% in T-section beams. In the model in [14], the contribution of cracked concrete zone is of secondary importance, it is from 13% to 36% in rectangular beams and from 7% to 17% in T-section beams. This is one of the reasons that the model in [13] underestimates the shear capacity of elements reinforced with GFRP bars, because due to the lower modulus of elasticity, the crack width calculated according to this model limits the possibility of the shear force transfer through the aggregate interlock in the shear crack.

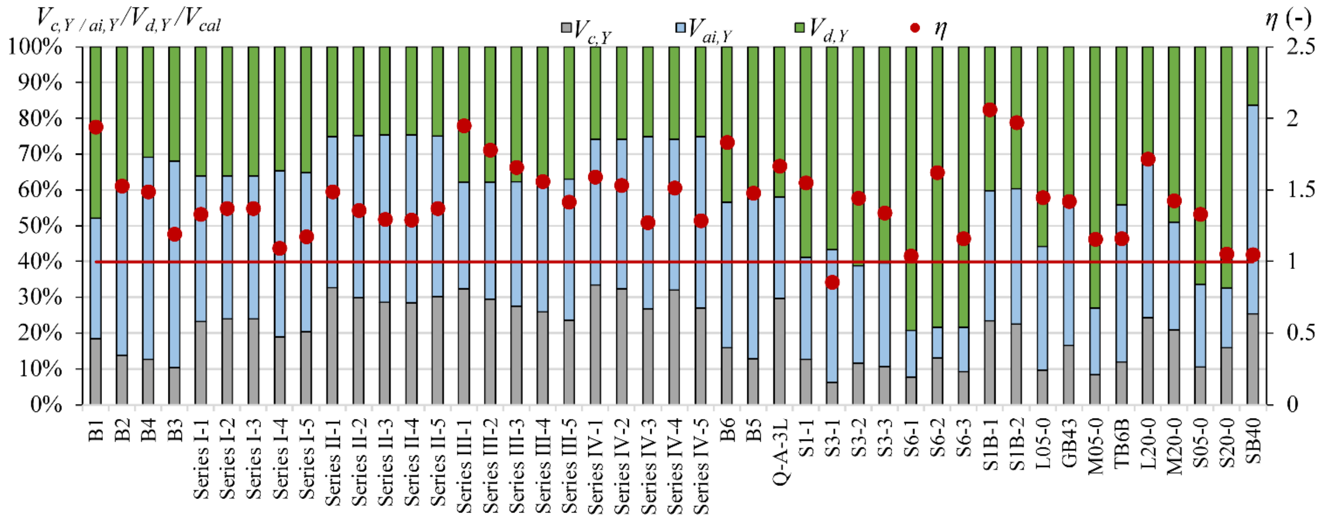

Figure 6. The comparison of shear mechanism contribution according to Yang's model for rectangular beams (red line indicated η = 1).

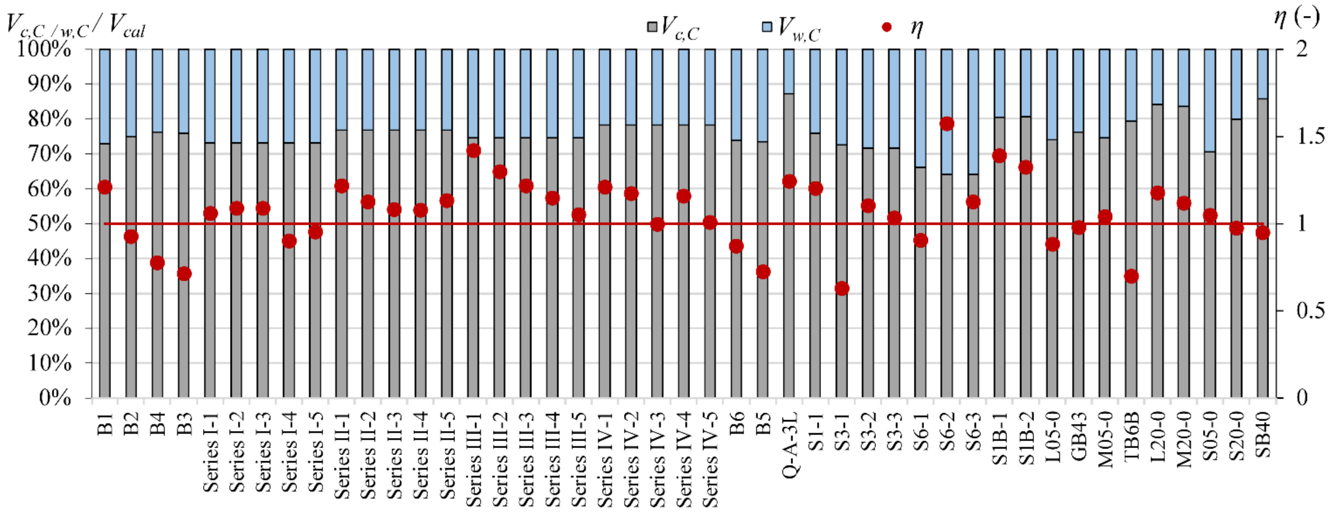

Figure 7. The comparison of shear mechanism contribution according to the Cladera et al. model for rectangular beams (red line indicated η = 1).

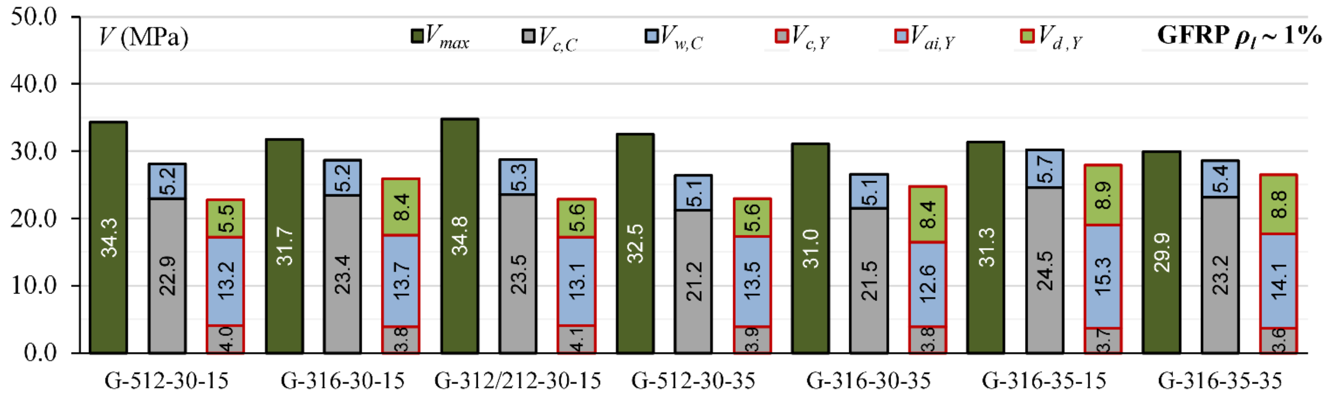

Figure 8. The comparison of shear mechanism contribution for GFRP-reinforced beams with reinforcement ratio ρ_l ~ 1% for Cladera et al.'s and Yang's models.

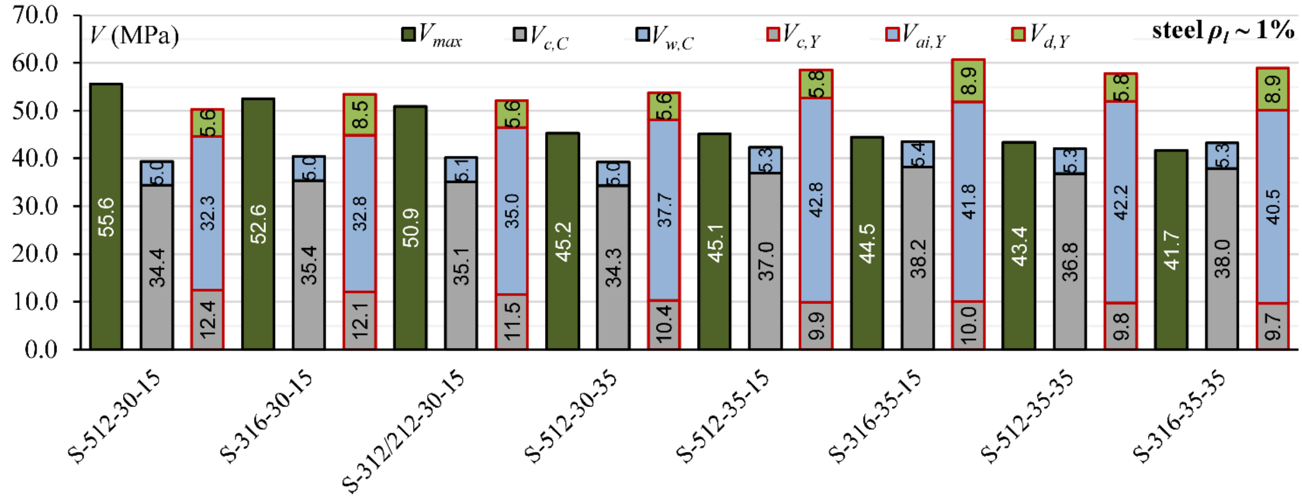

Figure 9. The comparison of shear mechanism contribution for steel-reinforced beams with reinforcement ratio ρ_l ~ 1% for Cladera et al.'s and Yang's models.

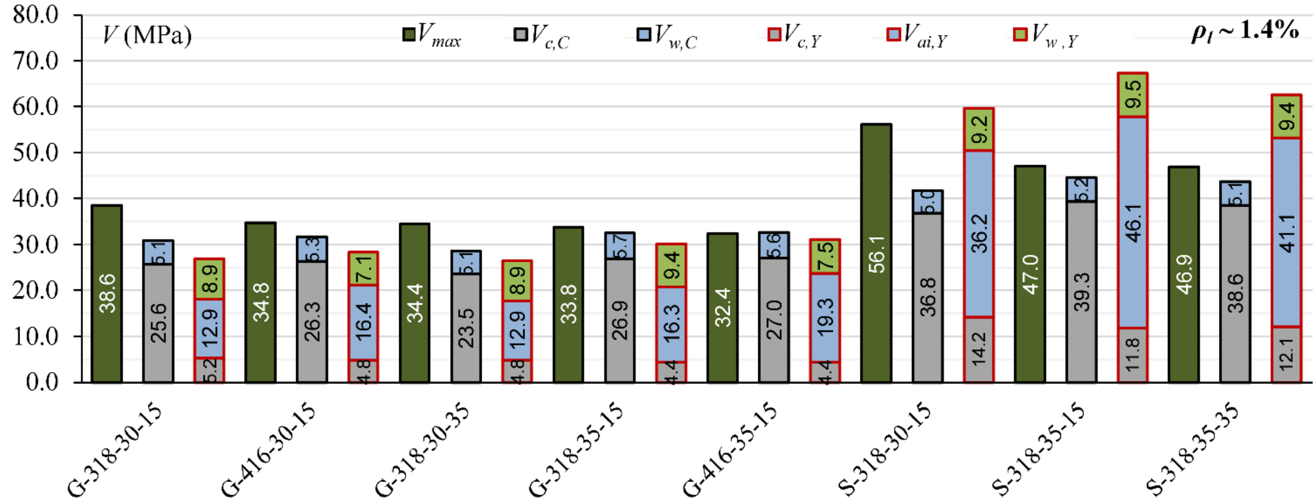

Figure 10. The comparison of shear mechanism contribution for GFRP and steel RC beams with reinforcement ratio ρ_l ~ 1.4% for Cladera et al.'s and Yang's models.

According to Yang's model, the contribution of the dowel effect is at the same level as the non-cracked concrete zone or even higher (Figure 6). In Cladera et al.'s model, the excluding of the dowel effect and assumption of the non-cracked concrete zone as the main shear transfer mechanism gives better accuracy. However, in Yang's model, the way of calculation of aggregate interlock based on Walraven's method seems very interesting. In both models, the individual contributions are independent, so a possible direction to improve Yang's model accuracy would be to disregard the dowel action contribution and consider the contribution of the non-cracked concrete zone according to Cladera et al.'s model. The results of these changes are visible in Figures 12 and 13. This uncomplicated modification decreases conservatism of Yang's model. However, especially in steel members, the calculated shear capacity is overestimated in reference to experimental results. This possible direction of modification must be verified in a higher number of elements.

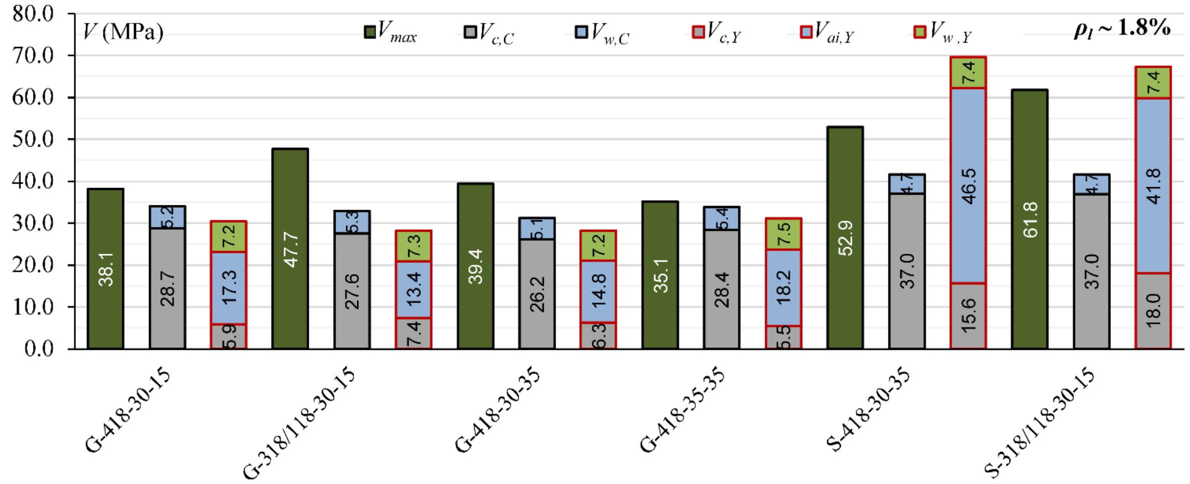

Figure 11. The comparison of shear mechanism contribution for GFRP and steel RC beams with reinforcement ratio ρ_l ~ 1.8% for Cladera et al.'s. and Yang's models.

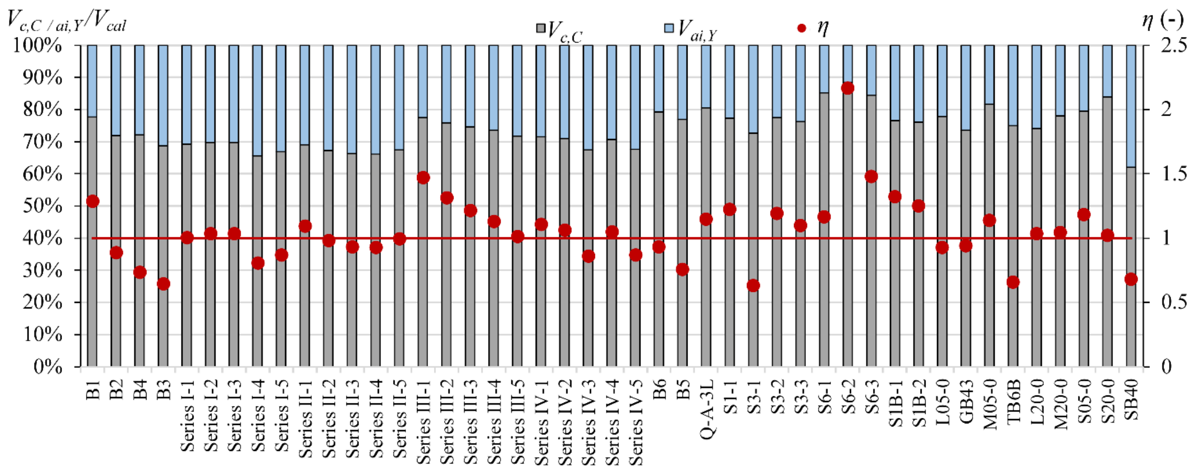

Figure 12. The shear capacity in rectangular beams for V_c from Cladera et al.'s. and V_{ai} from Yang's models (red line indicated η = 1).

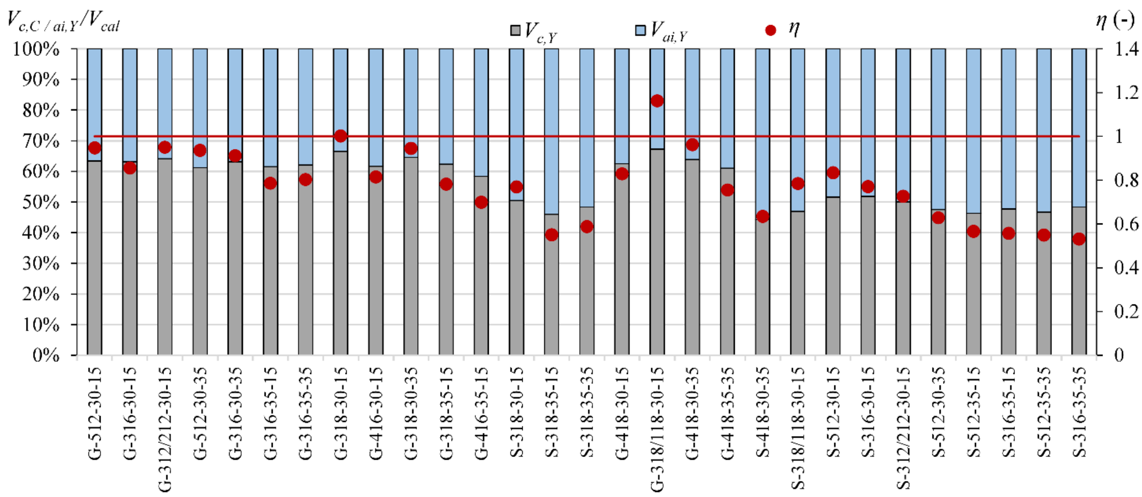

Figure 13. The shear capacity in T-section beams for V_c from Cladera et al.'s. and V_{ai} from Yang's models (red line indicated η = 1).

5. Conclusions

Based on the experimental and analytical results, the following conclusions can be drawn:

(1) Zhang et al.'s model [12] was dedicated to the beams without stirrups with variable types of longitudinal reinforcement. The shear capacity according to this model was calculated for the higher number of members than in the case of the remained models. However, it is shown an overestimation of this model in comparison with the experimental results in 49% analyzed beams. The detailed analysis crack propagation for T-section elements from our own research showed inconsistency for angle and location of critical crack in model and in tests. Unfortunately, there are too few data available in the literature from the database to calibrate these parameters.

(2) Yang's model [13] was originally established for steel-reinforced beams, so for the FRP-reinforced beams, the shear capacity was underestimated in comparison with the experimental values for a significant number of analyzed members. Interesting in this model is the possibility of calculation of the contribution of individual mechanism governed shear capacity (force transmitted by concrete, by aggregate interlock and by dowel action of longitudinal reinforcement).

(3) Cladera et al.'s model [14] also makes it possible to calculate the shear resistance provided by the non-cracked concrete zone and as one component by the aggregate interlock and residual tensile strength with excluding dowel action.

(4) The comparison the range of contribution individual shear mechanism in [13,14] and coefficient η showed that better compatibility of calculated and experimental shear strength is for model, which the main influence on shear strength assigns to the non-cracked concrete zone.

(5) In Muttoni and Ruiz's model [11], similar to in Yang's model [13], a bigger influence of aggregate interlock than uncracked concrete zone in shear resistance was assumed. In effect of this, both models are conservative for FRP-reinforced beams, because the lower modulus of elasticity of FRP bars decreases the aggregate interlock effect.

The best recommendation of the presented models for prediction of the shear capacity of FRP-reinforced concrete beams is quite difficult. The number of experimental results for GFRP-reinforced beams is still limited in comparison with the steel RC beams. Moreover, T-beams with GFRP reinforcement were tested only in the authors' own research program. Based on this experimental test data, the best prediction of the shear strength was obtained according to the model by Cladera et al. [14]. This model proved the lowest dispersion of results and simultaneously the coefficient η_m was equal 1.09. The undoubted advantage of this model is the straightforward formula and possibility of consideration of a T-section shape in the shear analysis.

Author Contributions: Conceptualization, methodology, writing—original draft preparation, R.K. and M.K.; data curation, M.K.; writing—review and editing, R.K. All authors have read and agreed to the published version of the manuscript.

Funding: This research received no external funding.

Institutional Review Board Statement: Not applicable.

Informed Consent Statement: Not applicable.

Data Availability Statement: All data, models, and code generated or used during the study appear in the submitted article.

Acknowledgments: The authors gratefully acknowledge the ComRebars Company who supplied the GFRP reinforcement for the experimental test.

Conflicts of Interest: The authors declare no conflict of interest. The funders had no role in the design of the study; in the collection, analyses, or interpretation of data; in the writing of the manuscript; or in the decision to publish the results.

Abbreviations

The following symbols are used in this paper:

a	the distance from the support to the loading force [mm]
b_w	the width of web in T-beams and the width in rectangular beams [mm]
d	the effective depth [mm]
d_g	the maximum aggregate size [mm]
f_c	the concrete compressive strength [MPa]
f_{ctm}	the mean concrete tensile strength [MPa]
h_f	the height of flange in T-beams [mm]
n	the number of bars in longitudinal reinforcement [-]
x	the neutral axis depth [mm]
A_l	the cross section longitudinal reinforcement [mm^2]
E	the modulus of elasticity of longitudinal reinforcement [MPa]
E_c	the modulus of elasticity of concrete [MPa]
M	the bending moment in the critical section [kNm]
V	the shear force in critical section [kN]
ε	the strain in concrete [-]
$\rho_l = \frac{A_l}{b_w d}$	the longitudinal reinforcement ratio [%]
ϕ	the diameter of longitudinal reinforcement [mm]

Appendix A

Table 1. Test database of experimental and calculated shear strength.

	Specimen/Symbol	a/d	b_w (mm)	d (mm)	f_c (MPa)	d_g (mm)	Type	ϕ (mm)	E (GPa)	A_l (mm^2)	ρ_l (%)	V_{max} (kN)	[MR]	[Z]	[Y]	[C]
Tureyen and Frosch [32]	V-A-1	3.4	457	360	40.3	-	AFRP	-	47.1	1579	1.0	115.6	-	105.5	-	-
	V-A-2	3.4	457	360	42.6	-	AFRP	-	130.0	3159	1.9	178.3	-	224.6	-	-
Zhao et al. [33]	I-No.1	3.00	150	250	34.3	-	CFRP	-	105.0	568	1.5	45.0	-	37.4	-	-
	II-No.6	3.00	150	250	34.3	-	CFRP	-	105.0	1136	3.0	46.0	-	49.1	-	-
	IV-No.15	3.00	150	250	34.3	-	CFRP	-	105.0	852	2.3	40.5	-	44.0	-	-
El- Sayed et al. [34]	CN-1.7	3.10	250	326	43.6	-	CFRP	12.7	134	1393	1.7	124.5	-	106.3	82.4	-
	CH-1.7	3.10	250	326	63.0	-	CFRP	15.9	135	1390	1.7	130.0	-	124.8	88.8	-
	CH-2.2	3.10	250	326	63.0	-	CFRP	15.9	135	1787	2.2	174.0	-	138.0	98.6	-
Jin et al. [35]	C-L-18-R1-1,2	3.10	200	215.5	33.6	-	CFRP	9	146.2	127	0.3	25.8	-	25.9	25.4	-
	C-L-18-R2-1,2	3.10	150	215.5	33.6	-	CFRP	9	146.2	127	0.4	18.9	-	22.1	22.9	-
	C-L-18-R3-1,2	3.10	150	213.5	33.6	-	CFRP	13	147.9	265	0.8	15.3	-	28.6	38.6	-
	C-L-27-R1-1,2	3.10	200	215.5	40.3	-	CFRP	9	146.2	127	0.3	23.2	-	27.9	28.9	-
	C-L-27-R2-1,2	3.10	150	215.5	40.3	-	CFRP	9	146.2	127	0.4	21.1	-	23.8	23.4	-
	C-L-27-R3-1,2	3.10	150	213.5	40.3	-	CFRP	13	147.9	265	0.8	26.2	-	30.8	30.7	-
Razaqpur et al. [36]	B1	3.50	300	200	52.3	20	CFRP	9.5	114	213	0.4	64.0	36.4	40.7	33.0	52.9
	B2	3.50	300	300	52.3	20	CFRP	9.5	114	284	0.3	61.0	51.6	57.8	39.9	65.8
	B4	3.50	300	500	52.3	20	CFRP	9.5	114	425	0.3	68.0	72.6	91.8	45.7	87.4
	B3	3.50	300	400	52.3	20	CFRP	9.5	114	354	0.3	55.0	70.8	74.8	46.1	77.2
Razaqpur et al. [37]	BA3	3.56	200	225	40.5	-	CFRP	8	145	201	0.4	47.0	-	34.0	26.0	-
	BA4	4.50	200	225	40.5	-	CFRP	8	145	201	0.4	38.5	-	34.0	25.3	-
Ashour and Kara [38]	B-300-2	3.60	200	276.117	29.8	-	CFRP	7.5	141.44	88	0.2	32.9	-	22.8	16.1	-
	B-300-4	3.60	200	276.117	29.8	-	CFRP	7.5	141.44	177	0.3	32.9	-	31.4	22.9	-
Olivito and Zuccarello [39]	Series I-1	5.71	150	175	19.2	20	CFRP	10	115	236	0.9	19.5	18.0	18.1	14.6	18.4
	Series I-2	5.71	150	175	19.2	20	CFRP	10	115	236	0.9	20.0	17.8	18.1	14.6	18.4
	Series I-3	5.71	150	175	19.2	20	CFRP	10	115	236	0.9	20.0	17.8	18.1	14.6	18.4
	Series I-4	5.71	150	175	19.2	20	CFRP	10	115	236	0.9	16.6	19.6	18.1	15.2	18.4
	Series I-5	5.71	150	175	19.2	20	CFRP	10	115	236	0.9	17.6	19.0	18.1	15.0	18.4
	Series II-1	5.71	150	175	19.2	20	CFRP	10	115	393	1.5	26.0	20.9	22.3	17.5	21.3
	Series II-2	5.71	150	175	19.2	20	CFRP	10	115	393	1.5	24.0	21.6	22.3	17.7	21.3
	Series II-3	5.71	150	175	19.2	20	CFRP	10	115	393	1.5	23.1	22.0	22.3	17.8	21.3
	Series II-4	5.71	150	175	19.2	20	CFRP	10	115	393	1.5	23.0	22.0	22.3	17.8	21.3
	Series II-5	5.71	150	175	19.2	20	CFRP	10	115	393	1.5	24.2	21.6	22.3	17.6	21.3
	Series III-1	5.71	150	175	25.6	20	CFRP	10	115	236	0.9	29.9	16.2	20.2	15.3	21.3
	Series III-2	5.71	150	175	25.6	20	CFRP	10	115	236	0.9	27.3	17.1	20.2	15.3	21.0
	Series III-3	5.71	150	175	25.6	20	CFRP	10	115	236	0.9	25.6	17.8	20.2	15.4	21.0
	Series III-4	5.71	150	175	25.6	20	CFRP	10	115	236	0.9	24.2	18.4	20.2	15.5	21.0
	Series III-5	5.71	150	175	25.6	20	CFRP	10	115	236	0.9	22.2	19.3	20.2	15.7	21.0
	Series IV-1	5.71	150	175	25.6	20	CFRP	10	115	393	1.5	29.7	22.5	25.0	18.7	21.0
	Series IV-2	5.71	150	175	25.6	20	CFRP	10	115	393	1.5	28.7	22.8	25.0	18.7	24.5
	Series IV-3	5.71	150	175	25.6	20	CFRP	10	115	393	1.5	24.5	24.6	25.0	19.2	24.5
	Series IV-4	5.71	150	175	25.6	20	CFRP	10	115	393	1.5	28.4	22.9	25.0	18.7	24.5
	Series IV-5	5.71	150	175	25.6	20	CFRP	10	115	393	1.5	24.7	24.5	25.0	19.2	24.5
Ashour and Kara [38]	B-200-2	5.90	200	169.918	24.7	-	CFRP	7.5	141.44	88	0.3	17.6	-	16.3	14.2	
	B-200-4	5.90	200	169.918	24.7	-	CFRP	7.5	141.44	177	0.5	20.8	-	22.2	18.7	
Razaqpur et al. [36]	B6	6.00	300	400	52.3	20	CFRP	9.5	114	354	0.3	62.0	39.2	74.8	33.8	71.2
	B5	6.50	300	400	52.3	20	CFRP	9.5	114	354	0.3	51.0	43.0	74.8	34.5	70.4

Table 1. *Cont.*

	Specimen/ Symbol	a/d	b_w (mm)	d (mm)	f_c (MPa)	d_g (mm)	Type	ϕ (mm)	E (GPa)	A_l (mm²)	ρ_l (%)	V_{max} (kN)	[MR]	[Z]	[Y]	[C]
Gross et al. [40]	8-2-1	6.36	127	143	55.0	-	CFRP	6.3	139.0	60	0.3	14.3	-	12.2	10.1	-
	8-2-2	6.36	127	143	55.0	-	CFRP	6.3	139.0	60	0.3	12.9	-	12.2	10.5	-
	8-2-3	6.36	127	143	55.0	-	CFRP	6.3	139.0	60	0.3	14.7	-	12.2	10.1	-
	11-2-1	6.36	89	143	76.0	-	CFRP	-	139.0	60	0.4	8.8	-	11.5	-	-
	11-2-2	6.36	89	143	76.0	-	CFRP	-	139.0	60	0.4	11.7	-	11.5	-	-
	11-2-3	6.36	89	143	76.0	-	CFRP	-	139.0	60	0.4	8.9	-	11.5	-	-
	8-3-1	6.45	159	141	55.0	-	CFRP	9.5	139.0	130	0.5	19.8	-	19.5	15.9	-
	8-3-2	6.45	159	141	55.0	-	CFRP	9.5	139.0	130	0.5	23.1	-	19.5	15.5	-
	8-3-3	6.45	159	141	55.0	-	CFRP	9.5	139.0	130	0.5	17.0	-	19.5	16.5	-
	11-3-1	6.45	121	141	76.0	-	CFRP	-	139.0	130	0.6	14.3	-	19.0	-	-
	11-3-2	6.45	121	141	76.0	-	CFRP	-	139.0	130	0.6	15.3	-	19.0	-	-
	11-3-3	6.45	121	141	76.0	-	CFRP	-	139.0	130	0.6	16.6	-	19.0	-	-
Niewels [41]	Q-A-3L	2.93	300	444	43.3	8	GFRP	32	43.968	4021	3.3	149.0	92.5	137.6	89.3	119.9
El-Sayed et al. [34]	GN-1.7	3.10	250	326	43.6	-	GFRP	15.9	42	1390	1.7	77.5	-	65.0	45.4	=
	GH-1.7	3.10	250	326	63.0	-	GFRP	15.9	42	1390	1.7	87.0	-	75.8	50.0	=
	GH-2.2	3.10	250	326	63.0	-	GFRP	15.9	42	1787	2.2	115.5	-	84.8	52.8	=
Steiner et al. [42]	A1	3.1	457	889	29.6	-	GFRP	-	41.0	2413	0.6	159.0	-	172.1	-	-
Jin et al. [35]	G-L-18-R1-1,2	3.10	200	215.5	33.6	-	GFRP	9	41.0	127	0.3	20.7	-	14.3	14.8	-
	G-L-18-R2-1,2	3.10	150	215.5	33.6	-	GFRP	9	41.0	127	0.4	18.6	-	12.3	11.7	-
	G-L-18-R3-1,2	3.10	150	213.5	33.6	-	GFRP	13	40.0	265	0.8	15.3	-	16.0	17.3	-
	G-L-27-R1-1,2	3.10	200	215.5	40.3	-	GFRP	9	41.0	127	0.3	20.4	-	15.4	15.9	-
	G-L-27-R2-1,2	3.10	150	215.5	40.3	-	GFRP	9.00	41.0	127	0.4	20.0	-	13.3	12.2	-
	G-L-27-R3-1,2	3.10	150	213.5	40.3	-	GFRP	13.00	40.0	265	0.8	21.5	-	17.2	16.7	-
Matta et al. [43]	S3-0.24-1B	3.10	114	292	40.6	19	GFRP	-	48.2	393	1.2	22.0	26.5	23.5	-	25.2
	S3-0.24-2B	3.10	114	292	40.6	19	GFRP	-	48.2	393	1.2	20.6	27.6	23.5	-	25.2
	S6-0.24-1B	3.10	229	146	40.6	19	GFRP	-	48.2	395	1.2	33.0	31.6	23.6	-	32.6
	S6-0.24-2B	3.10	229	146	40.6	19	GFRP	-	48.2	395	1.2	32.5	31.9	23.6	-	32.6
Matta and Nanni [44]	S1-1	3.11	457	883	29.5	20	GFRP	32	40.7	2413	0.6	154.1	93.0	170.1	99.5	128.2
	S3-1	3.11	114	294	59.7	20	GFRP	16	40.8	201	0.6	15.2	23.2	18.9	17.7	24.1
	S3-2	3.11	114	294	32.1	20	GFRP	16	40.8	201	0.6	19.3	14.3	14.7	13.4	17.5
	S3-3	3.11	114	294	32.1	20	GFRP	16	40.8	201	0.6	18.1	15.0	14.7	13.5	17.5
	S6-1	3.11	229	147	59.7	20	GFRP	16	40.8	201	0.6	28.6	24.4	18.9	27.5	31.6
	S6-2	3.11	229	147	32.1	20	GFRP	16	40.8	201	0.6	36.8	14.9	14.7	22.7	23.4
	S6-3	3.11	229	147	32.1	20	GFRP	16	40.8	201	0.6	26.3	19.1	14.7	22.6	23.4
	S1B-1	3.12	457	880	29.5	20	GFRP	32	40.7	4825	1.2	220.7	126.2	234.0	107.1	158.7
	S1B-2	3.12	457	880	30.7	20	GFRP	32	41.4	4825	1.2	216.2	132.8	239.6	109.6	163.1
Ashour [45]	Beam 3	3.14	150	212	28.9	-	GFRP	12	32	226	0.7	17.5	-	13.0	13.2	11.3
	Beam 9	3.14	150	212	50.2	-	GFRP	12	32	339	1.1	27.5	-	19.6	16.1	18.1
Bentz et al. [46]	L05-0	3.26	450	937	46.0	10	GFRP	25.4	37	2152	0.5	135.0	75.5	190.5	93.2	152.7
	M05-0	3.48	450	438	35.0	10	GFRP	25.4	37	1076	0.5	86.0	45.9	82.3	74.5	82.6
	L20-0	3.56	450	857	36.0	10	GFRP	25.4	37	8608	2.2	232.0	134.6	309.2	135.2	196.8
	M20-0	3.77	450	405	35.0	10	GFRP	25.4	37	4304	2.4	138.0	94.0	148.0	96.8	123.2
	S05-0	3.93	450	194	35.0	10	GFRP	12.7	37	580	0.7	54.5	31.6	40.0	40.9	51.9
	S20-0	4.05	450	188	35.0	10	GFRP	25.4	37	2152	2.5	74.0	66.2	71.0	70.3	75.8
Guadagnini et al. [47]	GB43	3.36	150	223	40.3	20	GFRP	13.5	45	429	1.3	27.2	26.7	24.0	19.1	27.7
Tureyen and Frosch [32]	V-G1-1	3.4	457	360	39.7	-	GFRP	-	40.5	1579	1.0	108.9	-	97.9	-	-
	V-G2-1	3.4	457	360	39.8	-	GFRP	-	37.6	1579	1.0	95.4	-	94.7	-	-
	V-G1-2	3.4	457	360	42.2	-	GFRP	-	32.0	3159	1.9	138.0	-	123.5	-	-
	V-G2-2	3.4	457	360	42.5	-	GFRP	-	37.0	3159	1.9	153.7	-	132.1	-	-

Table 1. *Cont.*

	Specimen/ Symbol	a/d	b_w (mm)	d (mm)	f_c (MPa)	d_g (mm)	Type	ϕ (mm)	E (GPa)	A_l (mm^2)	ρ_l (%)	V_{max} (kN)	[MR]	[Z]	[Y]	[C]
Imjai [48]	TB6B	3.49	150	220	95.0	10	GFRP	13.5	45	429	1.3	29.1	30.2	34.0	25.1	41.6
Duranovic et al. [49]	GB2	3.65	150	210	38.1	-	GFRP	13.5	45	429	1.4	26.0	-	22.6	18.0	-
	GB6	3.65	150	210	32.9	-	GFRP	13.5	45	429	1.4	22.0	-	21.3	17.8	-
Ashour [45]	Beam 1	3.97	150	168	28.9	-	GFRP	6	38	113	0.4	12.5	-	9.0	8.6	-
	Beam 7	3.97	150	168	50.2	-	GFRP	12	32	339	1.3	17.5	-	17.3	15.5	-
Yost et al. [50]	1FRP-a	4.06	229	225	34.7	-	GFRP	19	40.336	567	1.1	39.1	-	30.9	28.9	-
	1FRP-b	4.06	229	225	34.7	-	GFRP	19	40.336	567	1.1	38.5	-	30.9	28.9	-
	1FRP-c	4.06	229	225	34.7	-	GFRP	19	40.336	567	1.1	36.8	-	30.9	29.0	-
	2FRP-a	4.06	178	225	34.7	-	GFRP	19	40.336	567	1.4	28.1	-	26.9	23.3	-
	2FRP-b	4.06	178	225	34.7	-	GFRP	19	40.336	567	1.4	35.0	-	26.9	23.0	-
	2FRP-c	4.06	178	225	34.7	-	GFRP	19	40.336	567	1.4	32.1	-	26.9	23.1	-
	3FRP-a	4.06	229	225	34.7	-	GFRP	19	40.336	851	1.7	40.0	-	37.0	30.4	-
	3FRP-b	4.06	229	225	34.7	-	GFRP	19	40.336	851	1.7	48.6	-	37.0	30.1	-
	3FRP-c	4.06	229	225	34.7	-	GFRP	19	40.336	851	1.7	44.7	-	37.0	30.1	-
	4FRP-a	4.06	279	225	34.7	-	GFRP	19	40.336	1134	1.8	43.8	-	46.9	38.0	-
	4FRP-b	4.06	279	225	34.7	-	GFRP	19	40.336	1134	1.8	45.9	-	46.9	37.8	-
	4FRP-c	4.06	279	225	34.7	-	GFRP	19	40.336	1134	1.8	46.1	-	46.9	37.7	-
	5FRP-a	4.08	254	224	34.7	-	GFRP	22	40.336	1140	2.0	37.7	-	44.5	37.9	-
	5FRP-b	4.08	254	224	34.7	-	GFRP	22	40.336	1140	2.0	51.0	-	44.5	37.0	-
	5FRP-c	4.08	254	224	34.7	-	GFRP	22	40.336	1140	2.0	46.6	-	44.5	37.1	-
	6FRP-a	4.08	229	224	34.7	-	GFRP	22	40.336	1140	2.2	43.5	-	42.0	33.7	-
	6FRP-b	4.08	229	224	34.7	-	GFRP	22	40.336	1140	2.2	41.8	-	42.0	33.8	-
	6FRP-c	4.08	229	224	34.7	-	GFRP	22	40.336	1140	2.2	41.3	-	42.0	33.8	-
El-Sayed et al. [34]	SN-1.7	3.10	250	326	43.6	-	steel	16	200	1407	1.7	144.5	-	124.7	101.1	-
	SH-1.7	3.10	250	326	63.0	-	steel	16	200	1407	1.7	160.0	-	146.5	110.3	-
	SH-2.2	3.10	250	326	63.0	-	steel	16	200	1810	2.2	184.0	-	161.0	125.7	-
Guadagnini et al. [47]	SB40	3.35	150	224	43.4	20	steel	12	207	452	1.3	45.3	50.2	48.3	43.2	47.8
Tureyen and Frosch [32]	V-S-1	3.4	457	360	40.9	-	steel	-	199.8	1579	1.0	180.5	-	198.6	-	-
	V-S-2	3.4	457	360	41.3	-	steel	-	200	3159	1.9	205.2	-	261.6	-	-
	V-D-2	3.4	457	360	43.6	-	steel	-	200	592	0.4	135.7	-	134.3	-	-
Yost et al. [50]	1Steel-a	4.03	229	227	34.7	-	steel	16	200	804	1.5	60.7	-	70.7	58.2	-
	1Steel-b	4.03	229	227	34.7	-	steel	16	200	804	1.5	56.3	-	70.7	59.3	-
	1Steel-c	4.03	229	227	34.7	-	steel	16	200	804	1.5	58.0	-	70.7	58.9	-
Olivito and Zuccarello [39]	S-1	5.56	150	180	19.2	20	steel	-	200	340	1.3	18.1	29.1	26.7	-	24.4

Table 1. *Cont.*

	Specimen/Symbol	a/d	b_w (mm)	d (mm)	f_c (MPa)	d_g (mm)	Type	ϕ (mm)	E (GPa)	A_l (mm^2)	ρ_l (%)	V_{max} (kN)	[MR]	[Z]	[Y]	[C]
	G-512-30-15	2.90	150	379	30.10	8	GFRP	12	50.5	565	0.99	34.27	25.92	40.81	22.73	28.09
	G-316-30-15	2.92	150	377	31.10	8	GFRP	16	50.5	603	1.07	31.75	29.13	42.49	25.91	28.63
	G-318-30-15	2.93	150	376	31.10	8	GFRP	18	50.5	763	1.35	38.57	30.24	46.93	26.97	30.86
	G-416-30-15	2.92	150	377	30.50	8	GFRP	16	50.5	804	1.42	34.77	33.57	47.67	28.25	31.52
	G-418-30-15	2.93	150	376	31.10	8	GFRP	18	50.5	1018	1.80	38.14	37.61	53.33	30.41	33.97
	G-312/212-30-15	2.99	150	367.8	32.30	8	GFRP	12	50.5	565	1.02	34.78	25.66	39.83	22.87	28.76
	G-318/118-30-15	3.00	150	367	32.30	8	GFRP	18	50.5	1018	1.85	47.72	32.14	51.50	28.19	32.88
Kotynia and Kaszubska [28]	G-512-30-35	3.06	150	359	31.10	8	GFRP	12	50.5	565	1.05	32.47	25.82	36.47	22.90	26.37
	G-316-30-35	3.08	150	357	30.50	8	GFRP	16	50.5	603	1.13	31.01	27.64	36.51	24.77	26.56
	G-318-30-35	3.09	150	356	30.50	8	GFRP	18	50.5	763	1.43	34.42	30.57	40.28	26.54	28.60
	G-418-30-35	3.09	150	356	30.10	8	GFRP	18	50.5	1018	1.91	39.41	34.19	45.25	28.26	31.23
	G-316-35-15	2.92	150	377	37.05	8	GFRP	16	50.5	603	1.07	31.31	32.04	48.35	27.92	30.24
	G-318-35-15	2.93	150	376	37.05	8	GFRP	18	50.5	763	1.35	33.76	36.13	53.43	30.15	32.56
	G-416-35-15	2.92	150	377	36.02	8	GFRP	16	50.5	804	1.42	32.43	38.13	53.97	31.17	32.66
	G-316-35-35	3.08	150	357	35.00	8	GFRP	16	50.5	603	1.13	29.90	30.34	40.26	26.48	28.59
	G-418-35-35	3.09	150	356	35.00	8	GFRP	18	50.5	1018	1.91	35.14	39.56	50.43	31.17	33.85
	S-512-30-15	2.90	150	379	31.10	8	steel	12	201	565	0.99	55.59	51.48	76.64	50.25	39.38
	S-316-30-15	2.92	150	377	32.30	8	steel	16	201	603	1.07	52.59	55.68	79.88	53.42	40.42
	S-318-30-15	2.93	150	376	33.80	8	steel	18	201	763	1.35	56.10	62.81	90.37	59.59	41.77
	S-312/212-30-15	2.99	150	367.8	32.30	8	steel	12	201	565	1.02	50.93	53.13	72.70	52.09	40.20
	S-318/118-30-15	3.00	150	367	33.80	8	steel	18	201	1018	1.85	61.79	68.51	94.37	67.21	41.64
	S-512-30-35	3.06	150	359	31.10	8	steel	12	201	565	1.05	45.24	53.90	66.21	53.67	39.16
Kotynia and Kaszubska [28]	S-418-30-35	3.09	150	356	33.80	8	steel	18	201	1018	1.91	52.94	70.18	86.62	69.58	41.66
	S-512-35-15	2.90	150	379	34.95	8	steel	12	201	565	0.99	45.14	60.21	83.90	58.50	42.36
	S-316-35-15	2.92	150	377	36.33	8	steel	16	201	603	1.07	44.52	63.55	87.47	60.67	43.55
	S-318-35-15	2.93	150	376	37.35	8	steel	18	201	763	1.35	47.04	70.69	97.62	67.35	44.55
	S-512-35-35	3.06	150	359	35.00	8	steel	12	201	565	1.05	43.40	58.10	72.27	57.74	42.13
	S-316-35-35	3.08	150	357	36.33	8	steel	16	201	603	1.13	41.72	61.90	75.09	59.03	43.31
	S-318-35-35	3.09	150	356	36.33	8	steel	18	201	763	1.43	46.89	66.23	81.85	62.60	43.70

[MR]—Muttoni and Ruitz; [Z]—Zhang et al.; [C]—Cladera et al.; [Y]—Yang.

References

1. FIB Task Group 9.3. FRP Reinforcement in RC Structures. Bulletin No. 40, 2007, p. 160. Available online: https://re.public.polimi.it/handle/11311/661443 (accessed on 28 September 2007).
2. JSCE. *Recommendation for Design and Construction of Concrete Structures Using Continuous Fiber Reinforcing Materials*; Japan Soc. of Civil Engineers: Tokyo, Japan, 1997; Volume 23.
3. *ACI 440.1R-15*; Guide for the Design and Construction of Structural Concrete Reinforced with FRP Bars. American Concrete Institute: Farmington Hills, MI, USA, 2015; p. 88. [CrossRef]
4. *CAN/CSA-S806-12*; Design and Construction of Building Structures with Fibre-Reinforced Polymers. Canadian Standards Association: Toronto, ON, Canada, 2012; p. 206.
5. *ISIS-M03-07*; Reinforcing Concrete Structures with Fiber Reinforced Polymers. Canadian Network of Centers of Excellence on Intelligent Sensing for Innovative Structures. ISIS Canada: Winnipeg, MB, Canada, 2007.
6. Kaszubska, M. Analysis of the Flexural Reinforcement on the Shear Strength of the Concrete Beams without Transverse Reinforcement. Ph.D. Thesis, Lodz University of Technology, Lodz, Poland, December 2018.
7. Taylor, H.P.J. *Investigation of the Dowel Shear Forces Carried by Tensile Steel in Reinforced Concrete Beams*; Technical Report no. TRA 431; Cement and Concrete Association: London, UK, November 1969.
8. Taylor, H.P.J. *Investigation of the Forces Carried Across Cracks in Reinforced Concrete Beams in Shear by Interlock of Aggregate*; Technical Report No. 42.77; Cement and Concrete Association: London, UK, 1970.
9. Tottori, S.; Wakui, H. Shear capacity of RC and PC beams using FRP reinforcement. *Proc. Aci Sp Detroit* **1993**, *138*, 615–632. [CrossRef]
10. Marí, A.; Bairán, J.; Cladera, A.; Oller, E.; Ribas, C. Shear-flexural strength mechanical model for the design and assessment of reinforced concrete beams. *Struct. Infrastruct. Eng.* **2015**, *11*, 1399–1419. [CrossRef]
11. Muttoni, A.; Ruiz, M.F. Shear strength of members without transverse reinforcement as function of critical shear crack width. *ACI Struct. J.* **2008**, *105*, 163–172. [CrossRef]
12. Zhang, T.; Oehlers, D.J.; Visintin, P. Shear Strength of FRP RC Beams and One-Way Slabs without Stirrups. *J. Compos. Constr.* **2014**, *18*, 5. [CrossRef]
13. Yang, Y. Shear Behaviour of Reinforced Concrete Members without Shear Reinforcement, a New Look at an Old Problem. Ph.D. Thesis, Delft University of Technology, Delft, The Netherlands, April 2014.
14. Cladera, A.; Marí, A.; Bairán, J.M.; Ribas, C.; Oller, E.; Duarte, N. The compression chord capacity model for the shear design and assessment of reinforced and prestressed concrete beams. *Struct. Concr.* **2016**, *17*, 1017–1032. [CrossRef]
15. Kani, M.W.; Huggins, M.W.; Wittkopp, R.R. *Kani on Shear in Reinforced Concrete*; Deptartment of Civil Engineering, University of Toronto: Toronto, ON, Canada, 1979.
16. Lucas, W.; Oehlers, D.J.; Ali, M. Formulation of a Shear Resistance Mechanism for Inclined Cracks in RC Beams. *J. Struct. Eng.* **2011**, *137*, 12. [CrossRef]
17. ACI 363. State-of-the-Art Report on High-Strength Concrete (ACI 363R-92). *ACI J. Proc.* **1992**, *363*, 92.
18. Bažant, Z.P.; Ohtsubo, H. Stability conditions for propagation of a system of cracks in a brittle solid. *Mech. Res. Commun.* **1977**, *4*, 353–366. [CrossRef]
19. Walraven, J. Aggregate Interlock: A Theoretical and Experimental Analysis. Ph.D. Thesis, Delft University of Technology, Delft, The Netherlands, October 1980.
20. Baumann, T.; Rüsch, H. *Versuche zum Studium der Verdübelungswirkung der Biegezugbewehrung eines Stahlbetonbalkens (Heft 210)*; Ernst and Sohn: Berlin, Germany, 1970.
21. Mörsch, E. *Concrete-Steel Construction*; Engineering News Publishing Company: London, UK, 1909.
22. Marí, A.; Cladera, A.; Bairán García, J.M.; Oller, E.; Ribas, C. Shear-flexural strength mechanical model for the design and assessment of reinforced concrete beams subjected to point or distributed loads. *Struct. Infrastruct. Eng.* **2014**, *8*, 337–353. [CrossRef]
23. Cladera, A.; Marí, A.; Ribas, C.; Bairán, J.; Oller, E. Predicting the shear-flexural strength of slender reinforced concrete T and I shaped beams. *Eng. Struct.* **2015**, *101*, 386–398. [CrossRef]
24. Szczech, D.; Kotynia, R. Effect of shear reinforcement ratio on the shear capacity of GFRP reinforced concrete beams. *Arch. Civ. Eng.* **2021**, *67*, 1.
25. Szczech, D.; Kotynia, R. Shear Tests on GFRP Reinforced Concrete Beams. In Proceedings of the MATEC Web of Conferences EDP Sciences, Lodz, Poland, 21–23 October 2020; Volume 323. [CrossRef]
26. Kaszubska, M.; Kotynia, R.; Barros, J.A.O. Influence of Longitudinal GFRP Reinforcement Ratio on Shear Capacity of Concrete Beams without Stirrups. *Procedia Eng.* **2017**, *193*, 361–368. [CrossRef]
27. Kaszubska, M.; Kotynia, R.; Barros, J.A.O.; Baghi, H. Shear behavior of concrete beams reinforced exclusively with longitudinal glass fiber reinforced polymer bars: Experimental research. *Struct. Concr.* **2017**, *19*, 152–161. [CrossRef]
28. Kotynia, R.; Kaszubska, M. Research of the flexural reinforcement effect on the shear strength of concrete beams without transverse reinforcement. *Report* **2020**, *23*, 164.
29. *EN 1992-1-1*; Eurocode 2: Design of Concrete Structures. Part 1: General Rules and Rules for Buildings. British Standard Institution: London, UK, 2004.

30. Zhang, T.; Visintin, P.; Oehlers, D.J. Shear strength of RC beams without web reinforcement. *Aust. J. Struct. Eng.* **2016**, *17*, 87–96. [CrossRef]
31. Kupfer, H. *Erweiterung der Mörsch'schen Fachwerkanalogie mit Hilfe des Prinzips vom Minimum der Formänderungsarbeit*; CEB Bulletin d'information: Paris, France, 1964.
32. Tureyen, A.K.; Frosch, R.J. Shear tests of FRP-reinforced concrete beams without stirrups. *ACI Struct. J.* **2002**, *99*, 427–434. [CrossRef]
33. Zhao, W.; Maruyama, K.; Suzuki, H. Shear behaviour of concrete beams reinforced by FRP rods as longitudinal and shear reinforcement. In Proceedings of the Non-Metallic (FRP) Reinforcement for Concrete Structures, Second International RILEM Symposium, Rilem, Ghent, 23–25 August 1995.
34. El-Sayed, A.K.; El-Salakawy, E.; Benmokrane, B. Shear Capacity of High-Strength Concrete Beams Reinforced with FRP Bars. *ACI Struct. J.* **2006**, *103*, 383–389.
35. Jin, M.H.; Jang, H.S.; Kim, C.H.; Baek, D.I. Concrete Shear Strength of Lightweight Concrete BEAM REINFORCED with FRP bar. In Proceedings of the APFIS, Seoul, Korea; 9–11 December 2009.
36. Razaqpur, A.; Shedid, G.M.; Isgor, B. Shear Strength of Fiber-Reinforced Polymer Reinforced Concrete Beams Subject to Unsymmetric Loading. *J. Compos. Constr.* **2011**, *15*, 500–512. [CrossRef]
37. Razaqpur, A.G.; Isgor, B.O.; Greenaway, S.; Selley, A. Concrete Contribution to the Shear Resistance of Fiber Reinforced Polymer Reinforced Concrete Members. *J. Compos. Constr.* **2004**, *8*, 452–460. [CrossRef]
38. Ashour, A.F.; Kara, I.F. Shear Capacity of FRP Reinforced Concrete Beams. In Proceedings of the FRPRCS-11, Guimarães, Portugal; 26–28 June 2013.
39. Olivito, R.S.; Zuccarello, F.A. On the shear behaviour of concrete beams reinforced by carbon fibre-reinforced polymer bars: An experimental investigation by means of acoustic emission technique. *Strain* **2010**, *46*, 5. [CrossRef]
40. Gross, S.P.; Dinehart, D.W.; Yost, J.R.; Theisz, P.M. Experimental tests of high-strength concrete beams reinforced with CFRP bars. In Proceedings of the 4th International Conference on Advanced Composite Materials in Bridges and Structures (ACMBS-4), Calgary, AB, Canada; 20–23 July 2004.
41. Niewels, J. Zum Tragverhalten von Betonbauteilen mit Faserverbundkunststoff-Bewehrung. Ph.D Thesis, Rheinisch-Westfälische Technische Hochschule Aachen, Aachen, Germany, November 2008.
42. Steiner, S.; El-Sayed, A.K.; Benmokrane, B. Shear Behaviour of Large-Size Beams Reinforced with Glass FRP Bars. In Proceedings of the Annual Conference—Canadian Society for Civil Engineering, Quebec, Canada, 10–13 June 2008.
43. Matta, F.; El-Sayed, A.K.; Nanni, A.; Benmokrane, B. Size effect on concrete shear strength in beams reinforced with fiber-reinforced polymer bars. *ACI Struct. J.* **2013**, *110*, 617–628.
44. Matta, F.; Nanni, A. Scaling of strength of FRP reinforced concrete beams without shear reinforcement. In Proceedings of the Fourth International Conference on FRP Composites in Civil Engineering (CICE2008), Zurich, Shwitzerland, 22–24 July 2008.
45. Ashour, A.F. Flexural and shear capacities of concrete beams reinforced with GFRP bars. *Constr. Build. Mater.* **2006**, *20*, 1005–1015. [CrossRef]
46. Bentz, E.C.; Massam, L.; Collins, M.P. Shear Strength of Large Concrete Members with FRP Reinforcement. *J. Compos. Constr.* **2010**, *14*, 637–646. [CrossRef]
47. Guadagnini, M.; Pilakoutas, K.; Waldron, P. Shear Resistance of FRP RC Beams: Experimental Study. *J. Compos. Constr.* **2006**, *10*, 464–473. [CrossRef]
48. Imjai, T. Design and Analysis of Curved FRP Composites as Shear Reinforcement for Concrete Structures. Ph.D. Thesis, The University of Sheffield, Sheffield, UK, 2007.
49. Duranovic, N.; Pilakoutas, K.; Waldron, P. Tests on Concrete Beams Reinforced with Glass Fibre Reinforced Plastic Bars. In Proceedings of the Third International Symposium on Non-Metallic (FRP) Reinforcement for Concrete Structures (FRPRCS-3), Sapporo, Japan, 14–16 October 1997.
50. Yost, J.R.; Gross, S.P.; Dinehart, D.W. Shear Strength of Normal Strength Concrete Beams Reinforced with Deformed GFRP Bars. *J. Compos. Constr.* **2001**, *5*, 268–275. [CrossRef]